TEM Journal. Volume 15, Issue 3, pages 2064-2077, ISSN 2217-8309, DOI: 10.18421/TEM153-01, August 2026.

Impact Element as a Dynamical Absorber for a Duffing Oscillator

Nudžejma Smajlović [1], Džanko Hajradinović [2]

[1] *Stamen Modules doo, Krivoglavci I-5 71000, Sarajevo, Bosnia and Herzegovina*
[2] *Faculty of Mechanical Engineering, University of Sarajevo, Sarajevo, Bosnia and Herzegovina*

***Abstract* – This paper analyzes the application of a vibro-impact element as a dynamic absorber for a Duffing oscillator. The Duffing oscillator is a nonlinear oscillator, modeled here as a single-degree-of-freedom system with a nonlinear spring. The complete system consists of a body performing translational oscillatory motion, a drive mechanism, a slider, a spring that connects the oscillator to the slider, and a vibro-impact element, in the form of the ball, that performs translational motion with impacts. For comparison, the response of the Duffing oscillator without the absorber is also analyzed. The differential equations of motion of both systems are derived using Lagrange's equations of the second kind, and solved numerically. The results are presented in the form of amplitude–frequency diagrams and time–displacement diagrams. It is shown that the amplitude of the main body is reduced when it is coupled with an impact element. The way in which this is affected by the stiffness of the spring, that connects the ball and Duffing oscillator, is presented. For selected excitation frequencies the basins of attraction of the ball are obtained. In this way, the set of possible initial conditions for which the system behaves like vibro-impact or purely oscillatory one, is determined.**

***Keywords* – Duffing oscillator, vibro-impact element, vibration.**

DOI: 10.18421/TEM153-01
https://doi.org/10.18421/TEM153-01

Corresponding author: Džanko Hajradinović,
Faculty of Mechanical Engineering, University of Sarajevo, Sarajevo, Bosnia and Herzegovina
Email: hajradinovic@mef.unsa.ba

Received: 08 December 2025.
Revised: 07 April 2026.
Accepted: 17 April 2026.
Published: 27 August 2026.

1. Introduction

Since machines were first developed and used, especially those powered by motors, vibration has been an unavoidable phenomenon. In order to understand and control vibration, it has been studied for many decades. This is particularly challenging in the case of nonlinear vibrations [1], [2]. A typical example of a nonlinear system is the Duffing oscillator. Different forms of the Duffing oscillator and their behavior under various conditions are presented by [3]. Over the time, new insights into the behavior of such an oscillator were obtained through both analytical and numerical analysis [4], [5]. This led to developing of different variants of methods, for both cases and for different nature of parameters, such as excitation type [6], [7].

Since the vibrations of the Duffing oscillator began to be analyzed, many studies have been conducted on different ways of attenuating them. The suppression of chaos in nonlinear oscillators using a linear vibration absorber was analyzed by [8], and, as a particular case, the suppression of chaos in a Duffing oscillator was studied. Just as a linear vibration absorber is used to attenuate the vibrations of the Duffing oscillator, the use of a suspended pendulum has also been analyzed [9]. A Duffing vibration absorber can also be used to reduce the vibrations of a Duffing oscillator [10]. This can be done with a passive or active Duffing vibration absorber. For an active vibration mitigation of a Duffing oscillator, inerter damper can also be used [11]. Impact dampers as vibration absorbers for different systems, including nonlinear systems, have been studied for many years [12]. The dynamical behavior of an electromechanical system with an impact element was studied by [13]. In their study, the role of the impact element was to attenuate the vibration of the main system, which was modeled as a Duffing oscillator.

An optimization analysis of vibro-impact damper parameters was conducted by [14], using standard MATLAB tools, and different sets of parameters were obtained. A vibro-impact element has also been analyzed as a nonlinear energy sink in the context of targeted energy transfer [15].

The optimization mechanism was studied under periodic and transient excitation. The dynamical behavior of an impact damper as a vibration absorber for a non-ideal system with a limited power supply was studied by [16]. During the impact between the impact element and the main system, different impact models can be applied. The effect of collision modeling on absorber efficiency was analyzed by [17]. They considered the Hooke–Newton, Hertz and Hunt–Crossley impact models and compared the system behavior in these cases. The effect of gravity and friction on the dynamics of an inclined vibro-impact nonlinear energy sink was addressed by [18]. The system considered was a linear oscillator coupled to a vibro-impact element acting as a nonlinear energy sink, and it was shown that the gravitational effect can be exploited in the design of the vibro-impact energy sink in order to improve its damping performance.

Impact dampers are widely applied and analyzed for the control of vibration in many industrial machines, their components and tools. A vibro-impact element as a nonlinear energy sink for chatter mitigation in turning processes was analyzed by [19]. The behavior of the system was investigated using asymptotic analysis, and an experimental procedure was also carried out, showing a reduction in the amplitude of the lathe tool. The application of vibro-impact dampers for the attenuation of brake squeal was analyzed by [20]. It was shown that audible squeal can be reduced by vibro-impacts of small masses embedded within the rotor.

When an impact element is added to the main system, the whole system becomes a vibro-impact system. Vibro-impact systems, as well as other dynamical systems, can be subjected to ideal or non-ideal excitation [21]. An important part of the analysis of these systems is the phase when impacts occur [22].

This analysis has become much easier due to software developments that enable better numerical simulations of such systems [23]. This paper presents an analysis of the behavior of a Duffing oscillator with an impact absorber.

The impact absorber is designed in the form of a ball connected to the main body (oscillator) by a spring. The impact element can perform translational motion with impacts, through which a reduction in the vibration amplitude of the main system is expected. The aim is to determine the vibration amplitudes of the main system with the absorber for jump-up and jump-down excitation frequencies, and to determine the initial conditions required for the ball to perform a specific regime of motion, either vibro-impact or purely oscillatory. The analysis is conducted for the steady state of the system and under ideal excitation.

The paper is divided into four sections. Section 2 describes the physical and mathematical models of the systems analyzed. Section 3 presents the results obtained by numerical analysis and the corresponding discussion. Section 4 provides conclusions on the effect of the vibro-impact element on the behavior of the Duffing oscillator.

2. Physical and Mathematical Models

The system analyzed in this paper consists of a Duffing oscillator (the main body whose motion is studied) and a vibro-impact element. To investigate the mitigation of the main body's vibration, a vibro-impact element in the form of a ball is attached to the oscillator by a spring, so that its impacts influence the motion of the oscillator. The oscillator is connected to a slider by a spring with a nonlinear characteristic, and the slider is, in turn, connected to a drive mechanism. The drive mechanism is driven by an electric motor operating at constant frequency. Since the motion of the system does not affect the excitation, the excitation is considered ideal. In addition to this system, a Duffing oscillator without a vibro-impact damper is also analyzed.

2.1. Physical Models

Physical model of the system analyzed in this paper is shown in Figure 1.

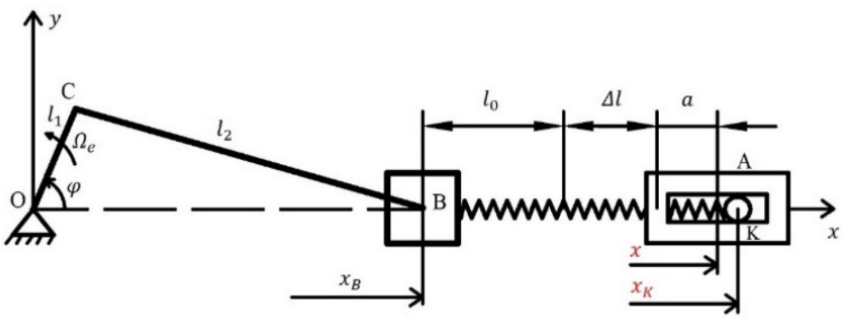

Figure 1. Physical model of Duffing oscillator with vibro-impact element

Body A represents the oscillator with mass m_A, which is the main body whose vibrations are supposed to be damped. On the oscillator, there is a ball with mass m_K, which is moving along and together with it. Ball is connected to oscillator with spring of stiffness c_1 and linear characteristics. The motion of the ball consists of the oscillatory motion and motion with impacts, that occur when the ball hits the inner wall of body A. Oscillator is connected to slider B with a spring which has nonlinear characteristics. The length of an undeformed spring is l_o, the stiffness of spring is c and its coefficient of nonlinearity is β. Slider B has a mass m_B and is driven by the excitation of the electric motor whose effect is transferred to drive mechanism, which transmits the movement to the other parts of the system. Drive mechanism consists of two rods, $\overline{OC}$ and $\overline{CB}$. Rod $\overline{CB}$ has a length l_2, mass m_2, moment of inertia J_2 (with respect to the axis through C) and is performing planar motion. Rod $\overline{OC}$ represents the drive rod with mass m_1, moment of inertia J_1 (with respect to the axis through O) and a length l_1. Drive rod is driven by electric motor with ideal excitation and is performing rotational motion.

Physical model of Duffing oscillator whose analysis is also conducted is the same like the above explained one, just without impact element on body A.

2.2. Mathematical Models

Equations of motion for the analyzed systems are formed by the application of Lagrange equations of type II. In the case of oscillatory system, as the system has one degree of freedom, only one differential equation is formed. For the vibro-impact system, two differential equations are formed.

2.2.1. Duffing Oscillator

Lagrange equation of type II for the described Duffing oscillator has a form:

$$\frac{d}{dt}\frac{\partial E_k}{\partial \dot{x}} - \frac{\partial E_k}{\partial x} = -\frac{\partial E_p}{\partial x} + Q_x \tag{1}$$

where E_k and E_p represent kinetic and potential energy of the system, respectively, x is generalized coordinate and Q_x is generalized force. Kinetic energy of the system represents the sum of kinetic energies of each individual body and can be written as follows:

$$E_k = E_{k_{p1}} + E_{k_{p2}} + E_{k_B} + E_{k_A} \tag{2}$$

$$E_k = \frac{1}{2}J_1\dot{\varphi}^2 + \frac{1}{2}m_2 v_{c_2}^2 + \frac{1}{2}J_2\omega_2^2 + \frac{1}{2}m_B\dot{x}_B{}^2 + \frac{1}{2}m_A\dot{x}^2 \tag{3}$$

where $\dot{\varphi}$ is the angular velocity of drive rod $\overline{OC}$, v_{C_2} is velocity of the center of inertia of rod $\overline{CB}$, ω_2 is the angular velocity of rod $\overline{CB}$ and x_B is the coordinate of slider B.

Function of the driving mechanism's motion $f(\varphi)$ is equivalent to the coordinate of slider, x_B:

$$\begin{gathered} x_B = f(\varphi) \\ \dot{x}_B = \frac{dx_B}{dt} = \frac{df(\varphi)}{dt} = \frac{d\varphi}{dt}\frac{df(\varphi)}{d\varphi} = \dot{\varphi}f'(\varphi) \end{gathered} \tag{4}$$

From the relations that are shown in Figure 1, x_B can be written as:

$$x_B = l_1 \cos\varphi + l_2\sqrt{1 + \frac{1}{2}\left(\frac{l_1}{l_2}\right)^2 (\cos 2\varphi - 1)} = f(\varphi) \tag{5}$$

Given that the system's excitation is ideal, the angular velocity $\dot{\varphi}$ is constant:

$$\dot{\varphi} = \Omega_e \tag{6}$$

Therefore, it can be written for angle φ:

$$\varphi = \int \dot{\varphi}\, dt = \Omega_e t + \varphi_0 \tag{7}$$

For the initial conditions applies:

$$\varphi_0 = \varphi(0) = 0 \tag{8}$$

then, it can be written:

$$\begin{gathered} \varphi = \Omega_e \cdot t = \Omega_p \cdot t \\ \ddot{\varphi} = 0 \end{gathered} \tag{9}$$

As the spring of the oscillator has a nonlinear characteristics potential energy of the system has a form:

$$E_p = \frac{1}{2}c(\Delta l)^2 + \frac{\beta}{4}(\Delta l)^4 \tag{10}$$

where Δl represents the deformation of the spring and can be expressed as:

$$\Delta l = x - x_B - l_0 - a = x - l_0 - a - f(\varphi) \tag{11}$$

After substitution of (11) into (10), the relation of potential energy of the system has a form:

$$E_p = \frac{c}{2}\big(x - l_0 - a - f(\varphi)\big)^2 + \frac{\beta}{4}\big(x - l_0 - a - f(\varphi)\big)^4 \tag{12}$$

The generalized force in this case is represented through the linear form of viscous friction:

$$Q_x = -b\dot{x} \tag{13}$$

After performing needed derivatives of equations (3) and (12), substituting them and equation (13) into (1), differential equation of motion of Duffing oscillator has a form:

$$\ddot{x}+\frac{b}{m_A}\dot{x}+\frac{c}{m_A}x+\frac{\beta}{m_A}\big(x-l_0-a-f(\varphi)\big)^3 = \frac{c}{m_A}l_0+\frac{c}{m_A}a+\frac{c}{m_A}f(\varphi) \tag{14}$$

2.2.2. Duffing Oscillator with Vibro-Impact Element

Compared to the Duffing oscillator, whose mathematical model was obtained firstly, in this case, the sum of the kinetic energies of the individual bodies also includes the kinetic energy of the ball K, so that the kinetic energy of a system is:

$$E_k=\frac{1}{2}J_1\dot{\varphi}^2+\frac{1}{2}m_2v_{c_2}^2+\frac{1}{2}J_2\omega_2^2+\frac{1}{2}m_B\dot{x}_B{}^2+\frac{1}{2}m_A\dot{x}^2+\frac{1}{2}m_K\dot{x}_K{}^2 \tag{15}$$

where x_K is the generalized coordinate of ball K.

In this case, the potential energy of the system has a form:

$$E_p=\frac{1}{2}c(\Delta l)^2+\frac{\beta}{4}(\Delta l)^4+\frac{1}{2}c_1(\Delta l_K)^2 \tag{16}$$

After defining the deformation Δl_K of the spring that connects body A and ball K, potential energy becomes:

$$E_p=\frac{c}{2}\big(x-l_0-a-f(\varphi)\big)^2+\frac{\beta}{4}\big(x-l_0-a-f(\varphi)\big)^4+\frac{c_1}{2}(x_K-x-l_K+a)^2 \tag{17}$$

Determining needed derivatives of equations of potential energy (17) and kinetic energy (15) for coordinates x and x_K and forms of generalized forces, equations of motion of body A and ball K, respectively, are defined as:

$$\ddot{x}+\frac{b}{m_A}\dot{x}+\frac{c-c_1}{m_A}x+\frac{\beta}{m_A}\big(x-l_o-a-f(\varphi)\big)^3 = \frac{c}{m_A}\big(f(\varphi)+l_0+a\big)+\frac{c_1}{m_A}(l_K-a-x_K) \tag{18}$$

$$\ddot{x}_K+\frac{b_1}{m_K}\dot{x}_K+\frac{c_1}{m_K}x_K=\frac{c_1}{m_K}(x+l_K-a) \tag{19}$$

For given systems for which mathematical models are mentioned above, numerical analysis is performed, with the help of given equations of motion through simulations in MATLAB. The analysis is conducted for steady state of motion of the systems.

2.3. Model of the Impact

During the impact of the ball K with the body A, the barrier is the inner wall of body A, as it is shown in Figure 2.

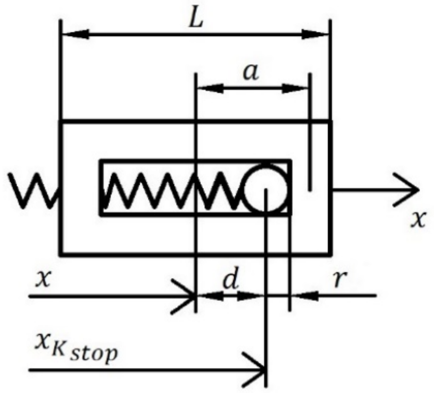

Figure 2. Position of the ball at the moment of impact

The coordinate of the ball can be written as:

$$x_{K_{stop}}=x+d \tag{20}$$

where d represents distance between the center of the ball and coordinate x, at the moment of impact and can be defined as:

$$d=\ a-\frac{L-2a}{2}-r \tag{21}$$

where L is the length of body A and r is the radius of the ball.

There are different cases when ball hits the oscillator depending on intensities and directions of velocities of them, both, before the impact, so that different cases of directions of velocities after the impact, are possible. This can be determined in different ways, depending on the used model of impact [24].

Based on the principle of conservation of momentum, it can be written:

$$m_A\vec{v}_A+m_K\vec{v}_K=m_A\vec{v}_A'+m_K\vec{v}_K' \tag{22}$$

where $\vec{v}_A$, $\vec{v}_K$ are the initial velocities and $\vec{v}_A', \vec{v}_K'$ are final velocities of body A and ball K respectively.

In order to determine relations of velocities of body A and ball K, four different possible cases will be considered, as shown in Figure 3.

The first case is when both, body A and ball K, are moving towards positive direction of x-axis before an impact, and after the impact ball is moving towards negative and oscillator towards positive direction of x-axis. Based on Newton's law of restitution, coefficient of restitution for first case can be expressed as:

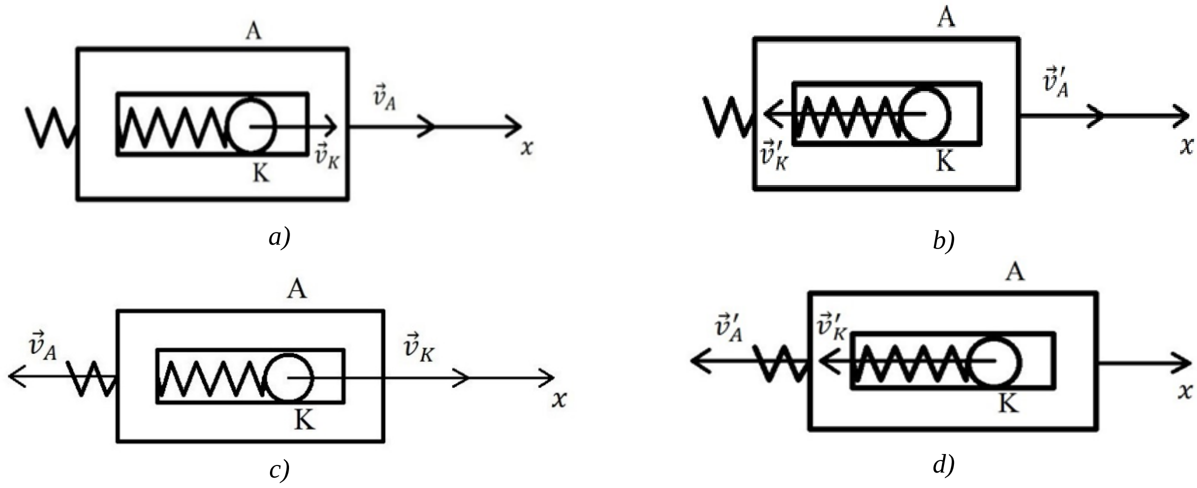

Figure 3. Directions of the velocities of bodies: a) case 1 and case 2 – before impact, b) case 1 and case 3 – after impact, c) case 3 and case 4 – before impact, d) case 2 and case 4 – after impact

$$k = \frac{-v_K' - v_A'}{v_A - v_K} \tag{23}$$

From the equation (23) velocities of the bodies after an impact can be written as:

$$v_A' = -v_K' - k(v_A - v_K) \tag{24}$$

$$v_K' = -v_A' - k(v_A - v_K) \tag{25}$$

By projecting expression (22) onto x-axis, for the case one, and combining it with equations (24) and (25), velocity of body A and ball K, after an impact become:

$$v_A' = \frac{v_A(m_A - m_K k) + m_K v_K(1+k)}{m_A + m_K} \tag{26}$$

$$v_K' = \frac{v_K(m_A k - m_K) - m_A v_A(1+k)}{m_A + m_K} \tag{27}$$

Velocities of the bodies, after an impact, for the other three cases are determined in the same way. Values of the system parameters used in conducted analysis are given in Table 1.

Table 1. System parameters

l_1	0.05	[m]	m_B	0.25	[kg]
l_2	0.15	[m]	m_K	0.02	[kg]
l_0	0.4	[m]	c	$9\pi^2$	[N/m]
l_K	0.02	[m]	c_1	$7\pi^2$	[N/m]
L	0.09	[m]	b	0.6	[Ns/m]
r	0.005	[m]	b_1	0.5	[Ns/m]
a	0.0375	[m]	β	75	[N/m^3]
m_A	0.4	[kg]	k	0.6	[-]

3. Results and Discussion

Numerical analysis of the described systems is performed with the help of MATLAB, by using differential equations and conditions of impact, obtained in previous section. The analysis was performed for steady state of the systems motion. Obtained results will be shown in the form of amplitude-frequency diagrams and time displacement diagrams.

3.1. Effect of a Vibro-Impact Element on the Behavior of Duffing Oscillator

Comparison of results obtained numerically for Duffing oscillator with and without vibro-impact element, is done with the aim of determining the influence of impact element on the oscillator´s behavior. For this purpose, there are amplitude-frequency diagrams of body A of Duffing oscillator, and body A of Duffing oscillator with vibro-impact element, for jump-up and jump-down frequencies, with labeled maximum displacement and natural frequency of the body, shown in Figure 4.

Results obtained for jump-up and jump-down frequencies are the same in the case of Duffing oscillator.

When the Duffing oscillator is coupled with vibro-impact element, the results are different. By numerical analysis it is possible to determine stable solutions, which are shown, on the mentioned diagrams, with red circles for jump-up, and blue circles for jump-down frequencies. The areas where the amplitude-frequency curve is parted, represent the areas of unstable solutions. Jumps that occur during this, are labeled with green arrows (Figure 4-a), 4-c)).

As the analyzed Duffing oscillator has one degree of freedom, on the amplitude-frequency diagram, one maximum can be noticed, while the slight elevation of the curve, on the left side from the maximum, is a consequence of sine and cosine functions present in differential equation of the system.

On the amplitude-frequency diagrams of Duffing oscillator with an impact element, there are two maxima, as the system has two degrees of freedom. It can be noticed that body A has lower maximum amplitude when Duffing oscillator is equipped with vibro-impact element, for both, jump-up and jump-down frequencies. It can be stated that the same can be concluded when the observation is done for both simulations together.

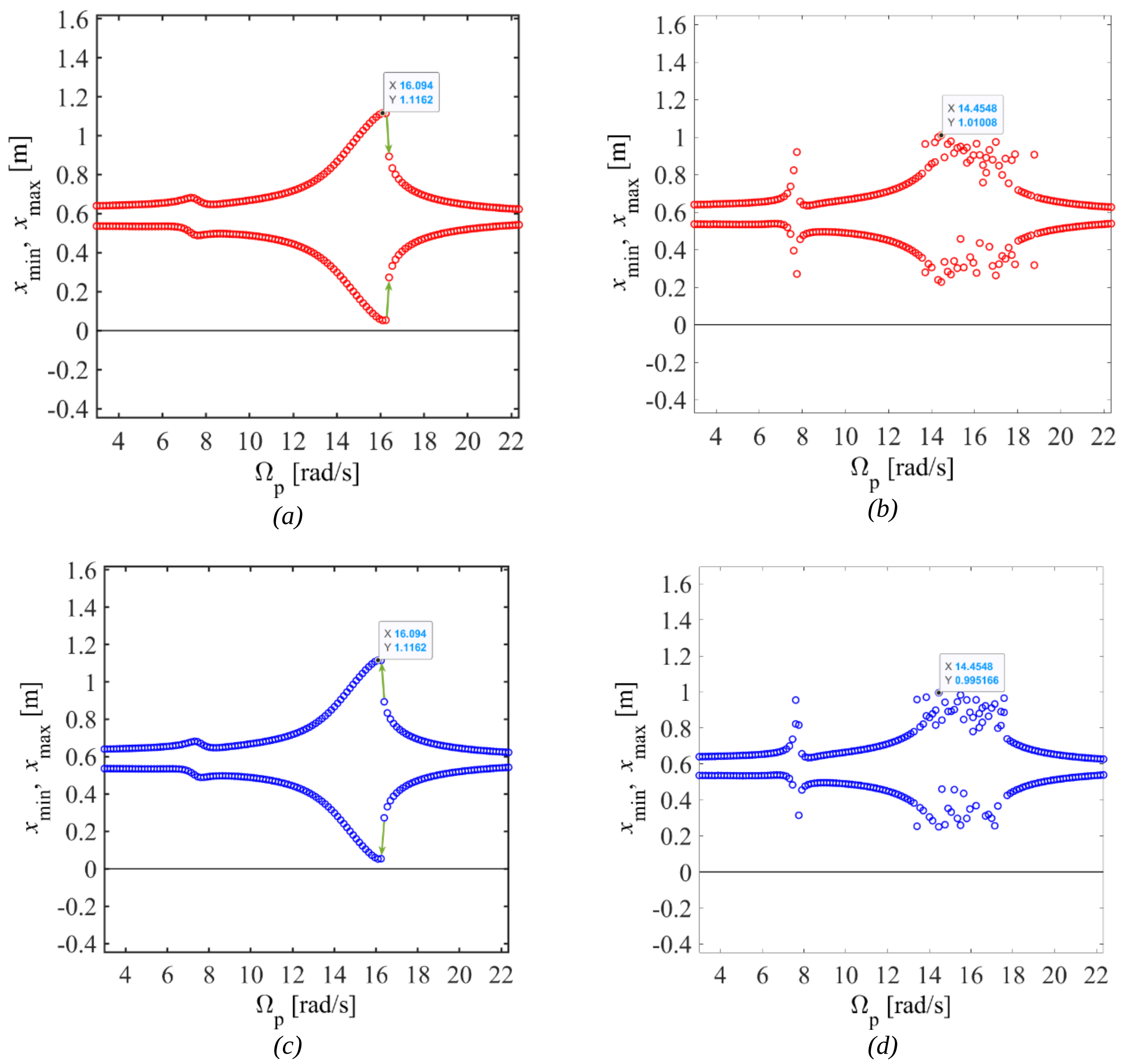

Figure 4. Amplitude-frequency diagrams of body A: a) Duffing oscillator: jump – up; b) Duffing oscillator with impact element: jump – up; c) Duffing oscillator: jump – down; d) Duffing oscillator with impact element: jump – down

Amplitude-frequency diagrams of Duffing oscillator with vibro-impact element have scatterings, that are not noticeable in the case of oscillator without impact element.

Time-displacement diagrams of body A of Duffing oscillator, and body A and ball K of Duffing oscillator with vibro-impact element, for the excitation frequency Ω_p = 7 rad/s, are shown in Figure 5.

In the period of time of 2000 s, it can be noticed that bodies are in steady state of motion. Diagrams, in the same figure, for last 30 s and 13 s of mentioned period of time, respectively, also demonstrate that.

The scattering observed in the amplitude-frequency diagrams of the Duffing oscillator with an impact element occurs only for certain excitation frequencies.

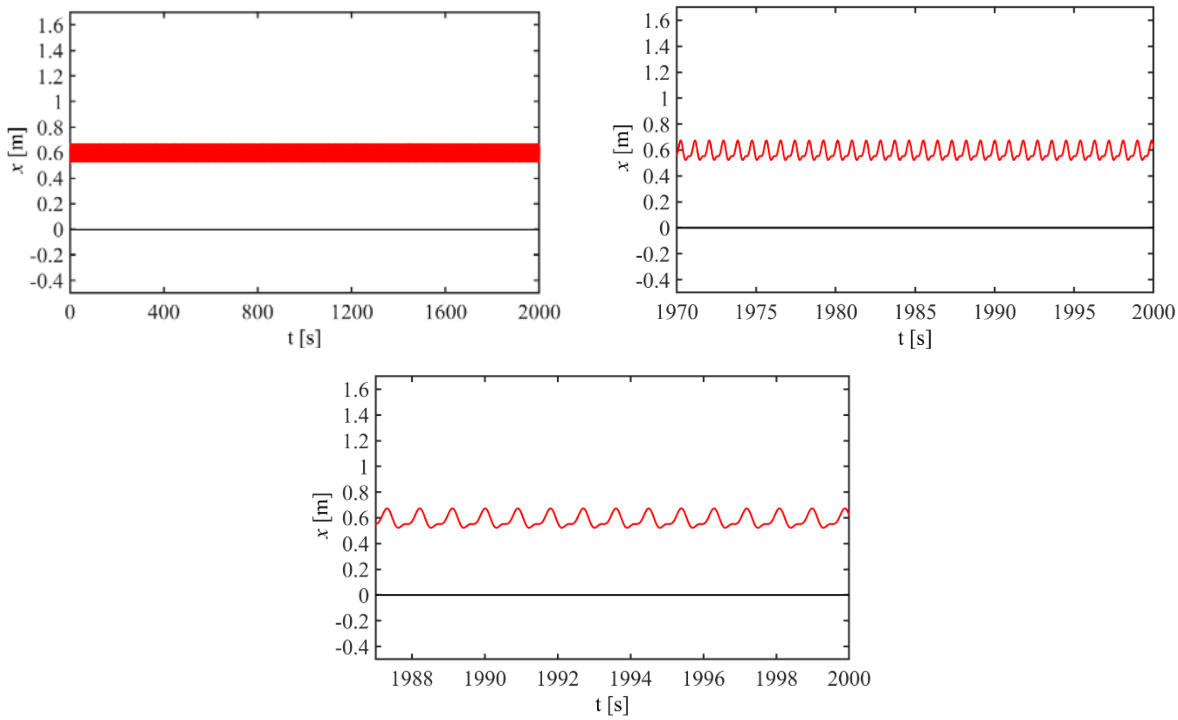

a)

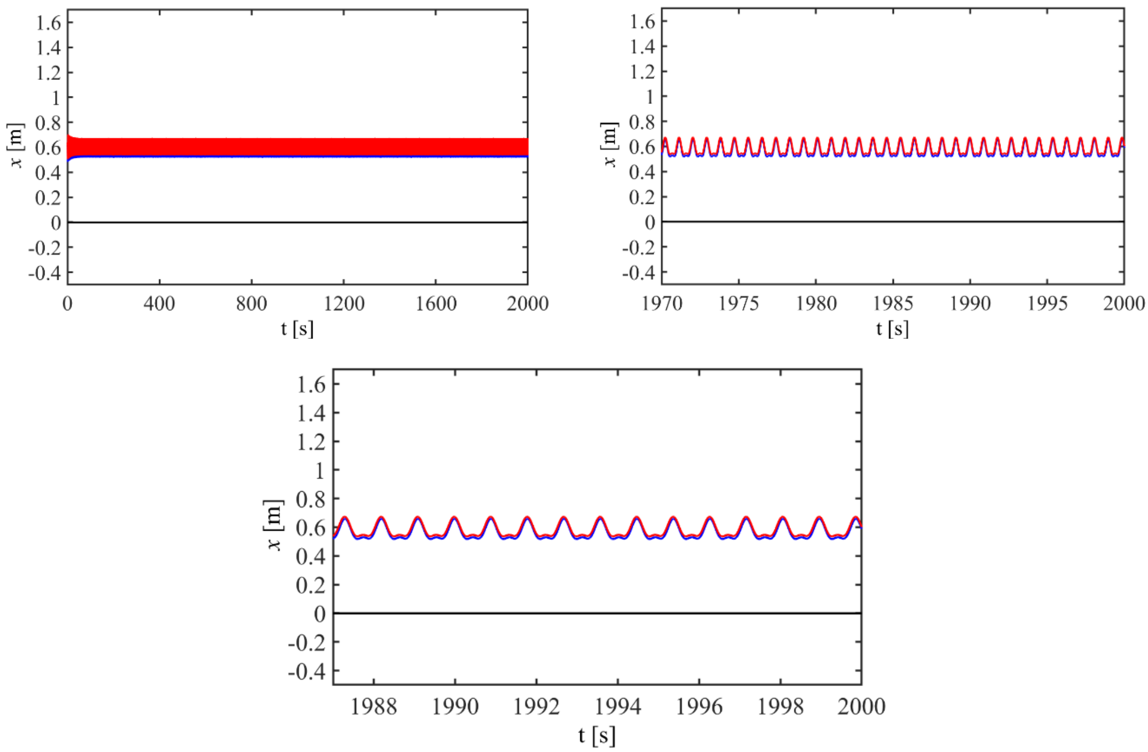

b)

Figure 5. Time – displacement diagrams, for Ω_p = 7 rad/s: a) of body A of Duffing oscillator, b) of body A (red) and impact element (blue) of Duffing oscillator with impact element

TEM Journal. Volume 15, Issue 3, pages 2064-2077, ISSN 2217-8309, DOI: 10.18421/TEM153-01, August 2026.

As Ω_p = 15 rad/s is one of the frequencies for which the scatterings occur, time-displacement diagrams of body A of Duffing oscillator and time-displacement diagrams of body A and ball K of Duffing oscillator with vibro-impact element, for this frequency, are shown in Figure 6.

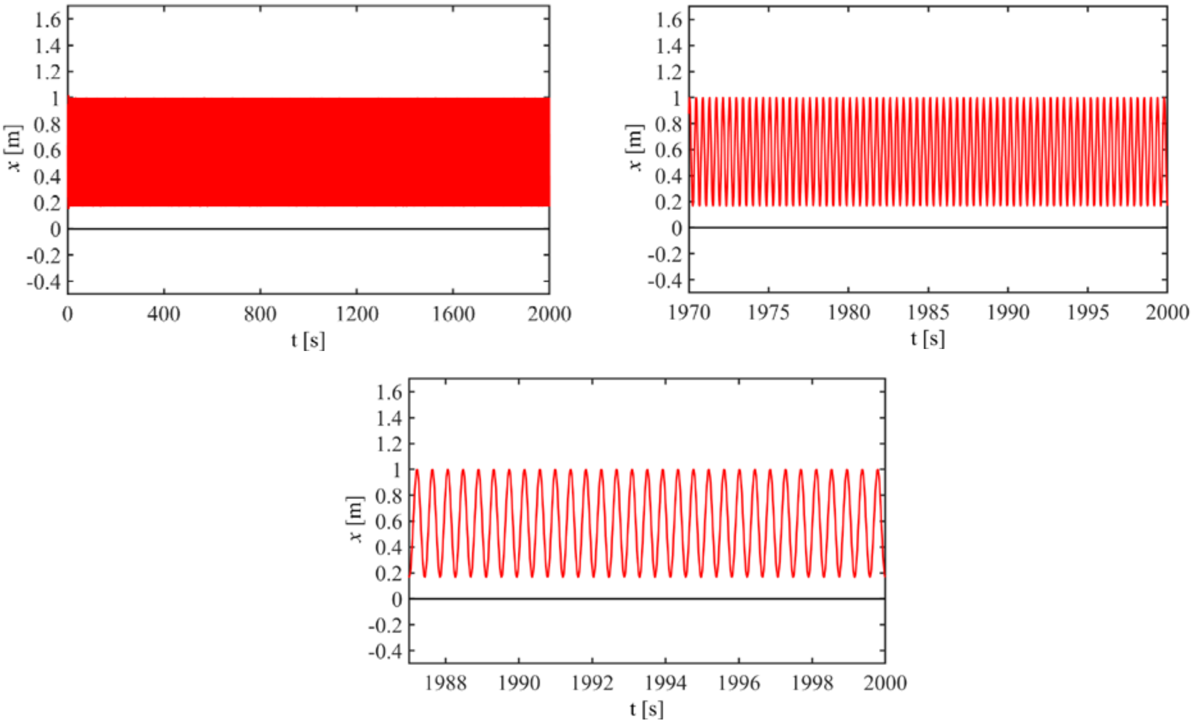

a)

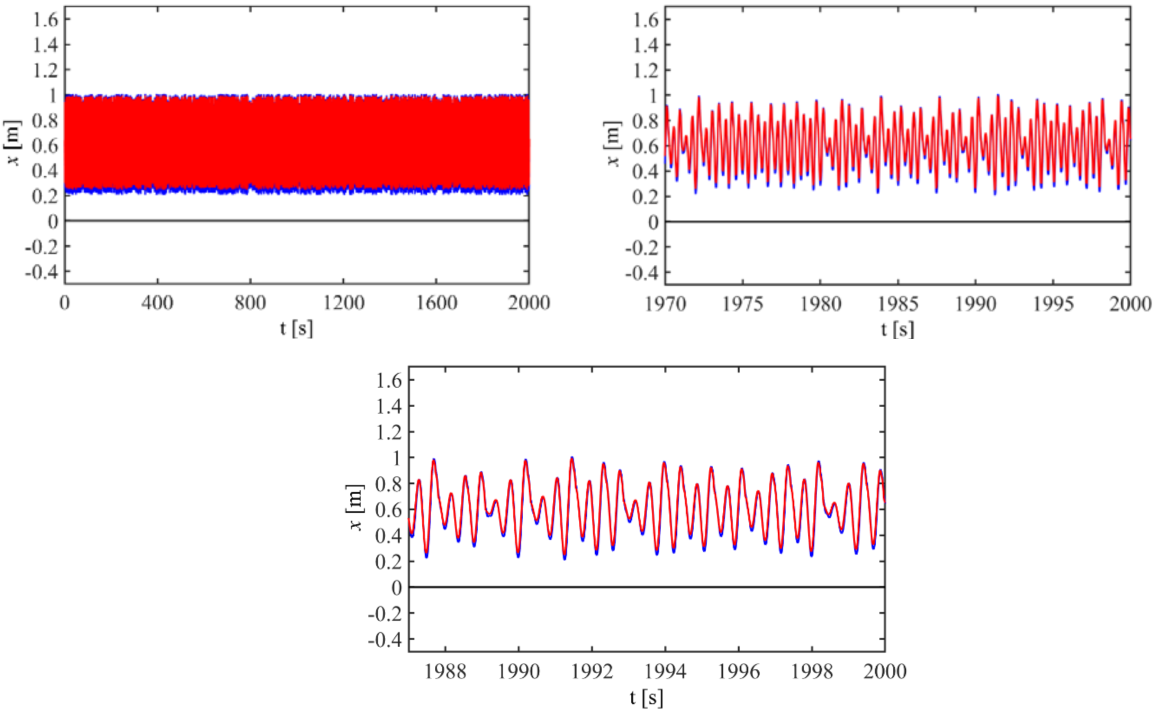

b)

Figure 6. Time – displacement diagrams for Ω_p = 15 rad/s: a) of body A of Duffing oscillator, b) of body A (red) and impact element (blue) of Duffing oscillator with impact element

By comparing mentioned diagrams, it can be noticed that there was a decrease in amplitudes of oscillations of body A, in the case of Duffing oscillator with an impact element.

In the case of Duffing oscillator, it reaches the steady state of motion very fast and much before 2000 s. Mentioned diagrams show that bodies did not reach the steady state of motion in 2000 s, when the oscillator is coupled with an impact element.

This may indicate that bodies reach the steady state later or that the motion of bodies is chaotic, in this case. In order to determine whether the motion of bodies is chaotic or bodies reach the steady state after 2000 s, time-displacement diagrams, for excitation frequency Ω_p = 15 rad/s and time of 5000 s are obtained.

Mentioned diagrams, for last 30 s and 13 s of 5000 s, respectively, are shown in Figure 7. It can be noticed that bodies are not oscillating in the steady state, also in this case.

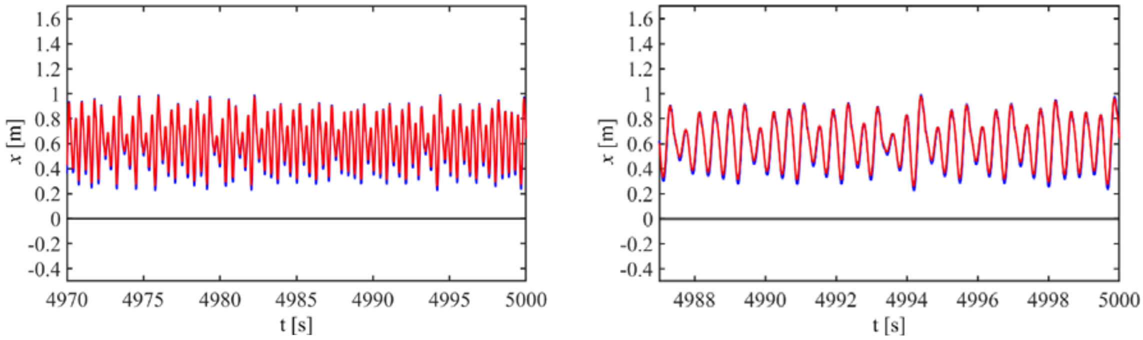

Figure 7. Time – displacement diagrams of body A (red) and impact element (blue) of Duffing oscillator with impact element, for Ω_p = 15 rad/s, and last period of 5000 s

To determine if bodies move chaotically, time-displacement diagrams are obtained, for the same excitation frequency, but the time of 9000 s. These diagrams, for last 30 s and 13 s of 9000 s, are shown in Figure 8.

It is noticed that bodies are not reaching steady state of motion in the time of 9000 s, also. Based on this, it can be stated that the motion of the oscillator and impact element is chaotic, for the frequencies for which scattering is obtained on amplitude-frequency diagrams.

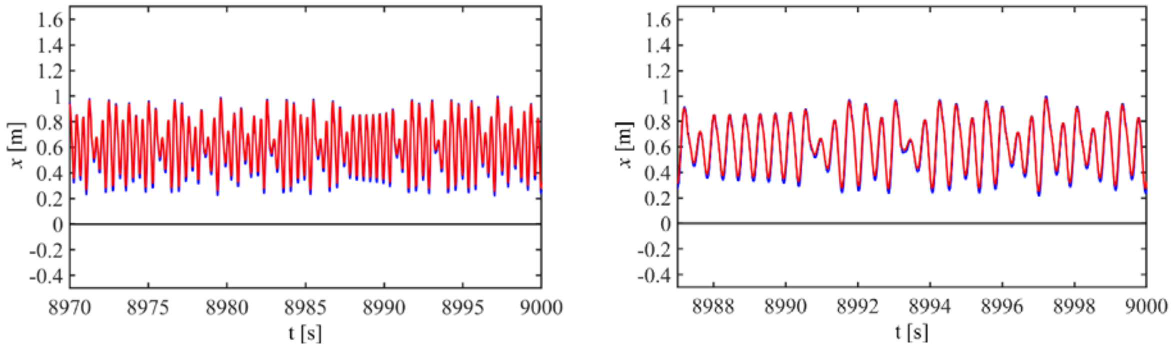

Figure 8. Time – displacement diagrams of body A (red) and impact element (blue) of Duffing oscillator with impact element, for Ω_p = 15 rad/s, and last period of 9000 s

At the moment when the ball hits the oscillator, on time-displacement diagrams of body A and impact element, the change of the shape of time-displacement curve can be noticed.

As this cannot be easily observed on time-displacement diagrams which are obtained for longer period of time, time-displacement diagram of body A and ball K of Duffing oscillator with vibro-impact element, for excitation frequency Ω_p = 15 rad/s, and for last 4 s of time of 2000 s, is shown in Figure 9.

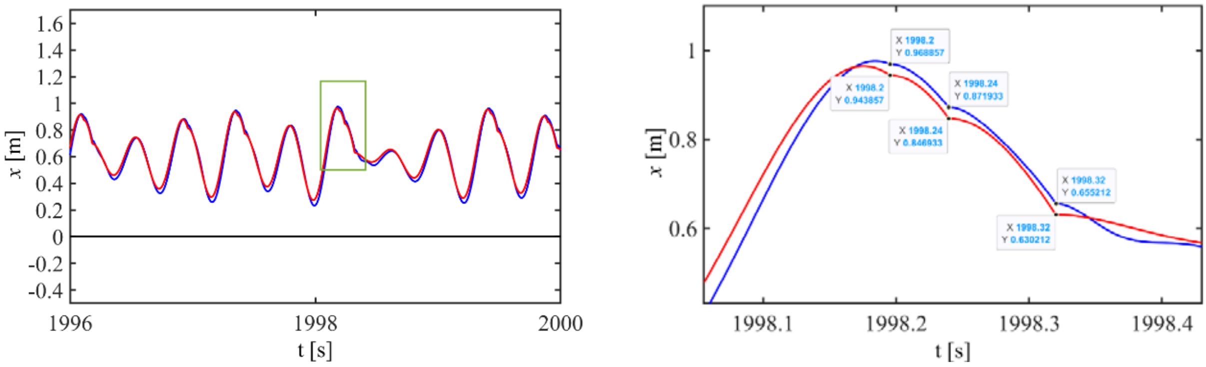

Figure 9. Time – displacement diagrams of body A (red) and impact element (blue) of Duffing oscillator with impact element, for Ω_p = 15 rad/s, and last 4s of 2000 s period of time: marked region-left, enlarged marked region with coordinates-right

On the region marked with green rectangle, three cases of mentioned changes of the shape of time-displacement curve can be noticed. Enlarged view of marked region is shown in Figure 9, on the right. In the same figure, there are shown coordinate values of body A and the ball, for mentioned cases of change in shape of time-displacement curve, at the moment of an impact. If the displacement coordinate value of body A is subtracted from the displacement coordinate value of the ball, the value of 0.025 m is obtained. This represents the value of parameter *d*, defined by equation (21), obtained by inserting parameter values defined in Table 1.

3.2. Effect of the Stiffness of Spring of a Vibro-Impact Element on the Behavior of Duffing Oscillator

The stiffness of a spring that connects vibro-impact element with an oscillator, represents the quantity that directly affects the occurrence of an impact. In the case of very stiff spring, a ball is not able to reach the wall of body A, so that impact will not even occur. With the aim of comparing behavior of Duffing oscillator for different values of stiffness of a spring of vibro-impact element, amplitude-frequency diagrams of body A of Duffing oscillator, for jump-up and jump-down frequencies are shown in Figure 10.

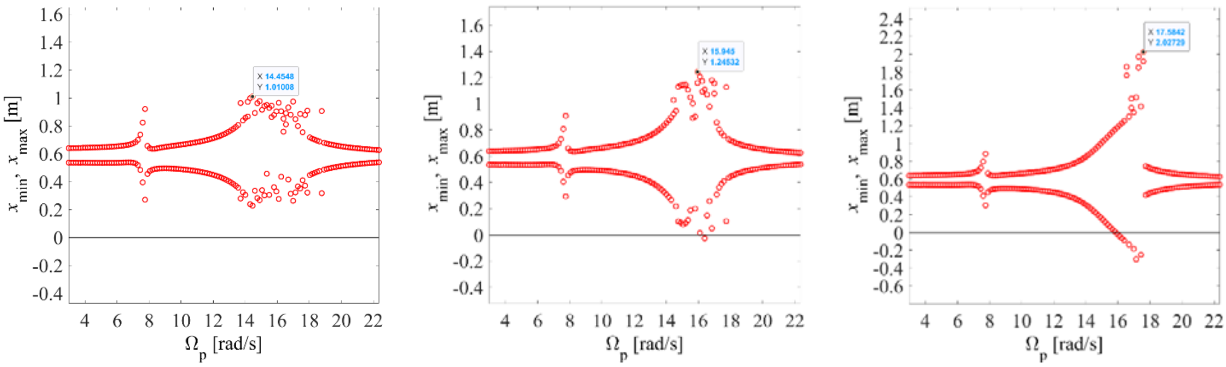

a)

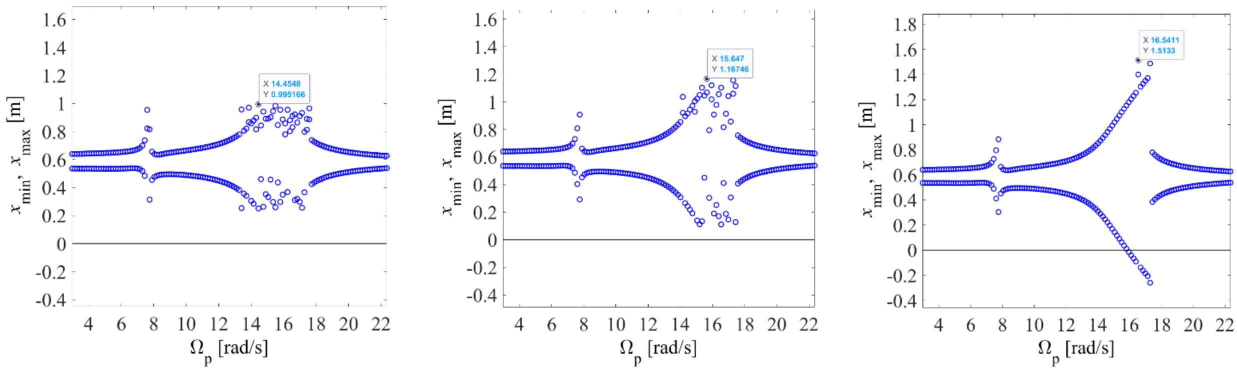

b)

Figure 10. Amplitude-frequency diagrams of body A, of Duffing oscillator with a vibro-impact element: a) jump – up: for $c_1 = 7\pi^2$ N/m, $c_1 = 11\pi^2$ N/m and $c_1 = 24\pi^2$ N/m; b) jump – down: for $c_1 = 7\pi^2$ N/m, $c_1 = 11\pi^2$ N/m and $c_1 = 24\pi^2$ N/m (respectively, from the left to the right)

Mentioned diagrams are obtained for three values of stiffness: $7\pi^2$ N/m, $11\pi^2$ N/m and $24\pi^2$ N/m. It is noticeable that maximum amplitude of body A, for jump-up frequencies, is the highest when the stiffness of the spring is $24\pi^2$ N/m, and the lowest for stiffness value of $7\pi^2$ N/m. In the case of jump-down frequencies, the highest maximum amplitude of the oscillator is noticed when the value of stiffness of the spring is $24\pi^2$ N/m, and the lowest one for the stiffness value of $7\pi^2$ N/m. If the simulations of jump-up and jump-down are observed together, maximum amplitude of the oscillator is the highest, when the stiffness of the spring is $24\pi^2$ N/m, and the lowest for the stiffness value of $7\pi^2$ N/m.

All of amplitude-frequency diagrams have regions of scatterings, and the narrowest one is for stiffness value of $24\pi^2$ N/m.

Time-displacement diagrams of body A and ball K, for mentioned values of stiffness of the spring, obtained for excitation frequency of Ω_p = 7 rad/s, are shown in Figure 11. For this frequency and stiffness values, body A and ball K, are oscillating in steady state. Obtained diagrams are the same, for mentioned parameters.

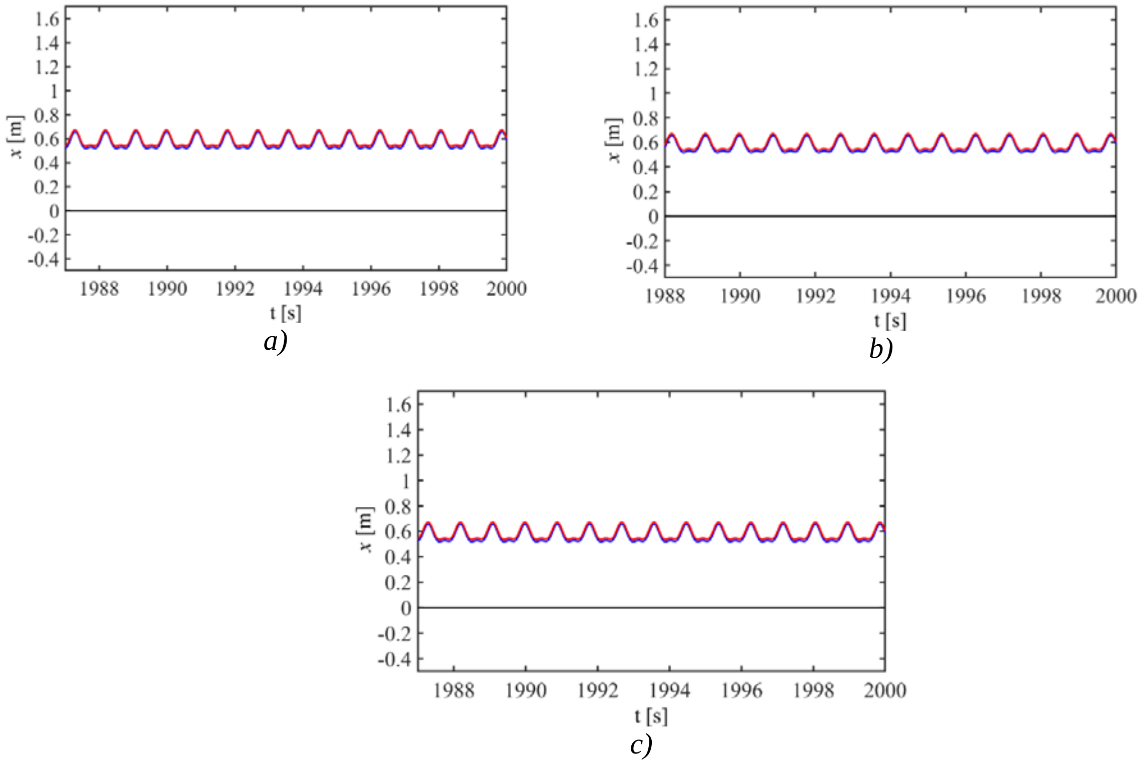

Figure 11. Time – displacement diagrams for Ω_p = 7 rad/s, of body A (red) and impact element (blue) of Duffing oscillator with a vibro-impact element: a) $c_1 = 7\pi^2$ N/m; b) $c_1 = 11\pi^2$ N/m; c) $c_1 = 24\pi^2$ N/m

Time-displacement diagrams of the oscillator and vibro-impact element are also obtained for excitation frequency of Ω_p = 17 rad/s, and shown in Figure 12. This excitation frequency is from the region of frequencies for which scatterings occur on amplitude-frequency diagrams (Figure 10).

That is why the motion of the oscillator is chaotic for this frequency, for every of three values of stiffness, which is shown by mentioned time-displacement diagrams.

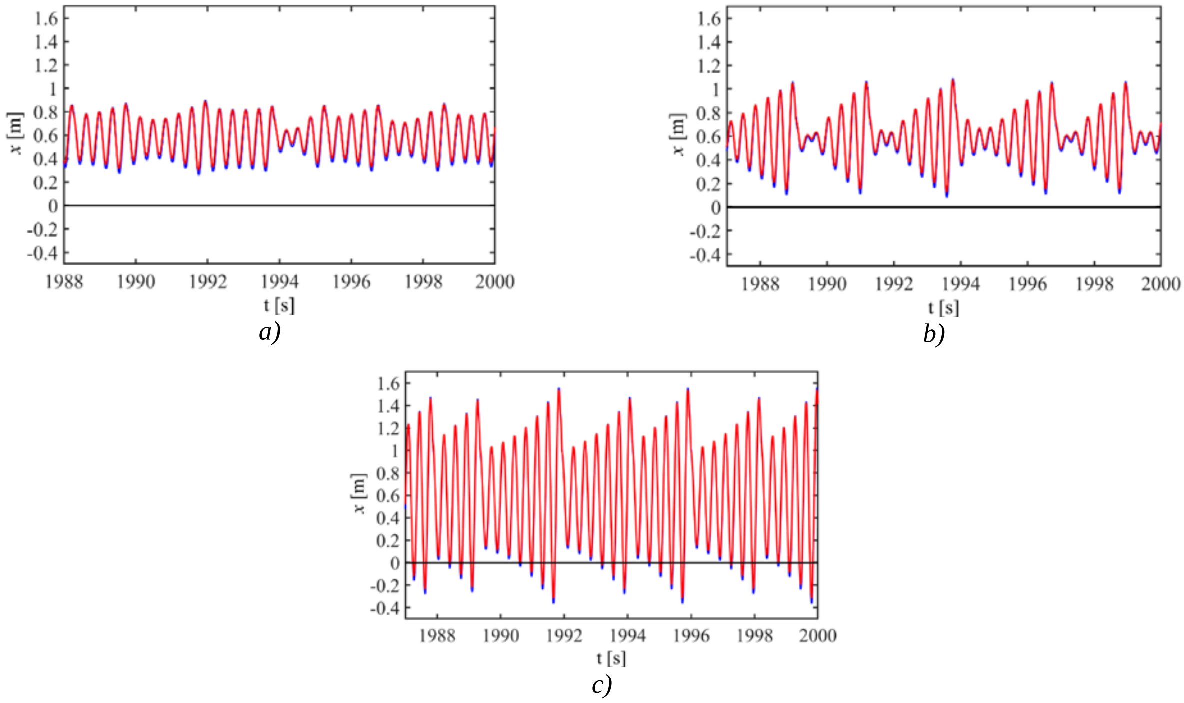

Figure 12. Time – displacement diagrams for Ω_p = 17 rad/s, of body A (red) and impact element (blue) of Duffing oscillator with a vibro-impact element: a) $c_1 = 7\pi^2$ N/m; b) $c_1 = 11\pi^2$ N/m; c) $c_1 = 24\pi^2$ N/m

3.3. Effect of Initial Conditions on the Behavior of Duffing Oscillator with Vibro-Impact Element

For different initial conditions of a body A and ball, the behavior of the system is different. Basins of attraction, for certain frequencies, are obtained, in order to determine for which initial conditions the system performs vibro-impact motion, and for which just oscillatory one. Amplitude-frequency diagrams, for jump-up and jump-down frequencies, of a vibro-impact element are shown in Figure 13.

There are noticeable scatterings, for some frequencies, as it was in the case of body A. As it was stated before, these scatterings indicate chaotic motion of a ball, for certain values of excitation frequency. In order to determine the effect of initial conditions on the behavior of Duffing oscillator, for the case of steady state and chaotic motion, basins of attraction are obtained for excitation frequency Ω_p = 16 rad/s and Ω_p = 22 rad/s, respectively.

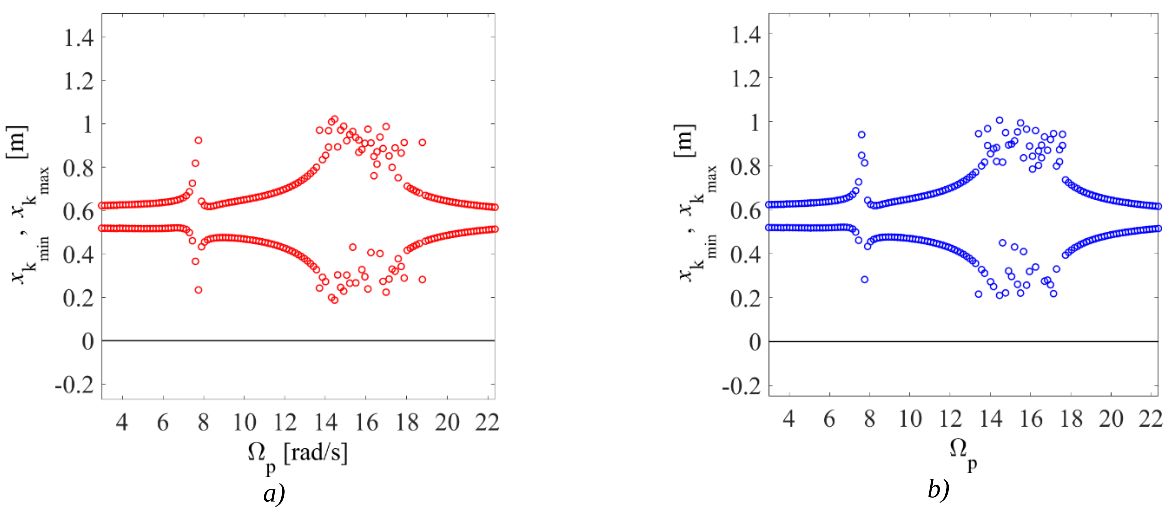

Figure 13. Amplitude-frequency diagrams of vibro-impact element: a) jump – up; b) jump – down

Basin of attraction, for frequency of excitation Ω_p = 16 rad/s, is shown in Figure 14.

Red regions are the regions of initial conditions for which the system behaves as oscillatory one. For the initial conditions from blue regions, the system is vibro-impact.

It is clearly noticeable that the red regions are narrow. These regions are also scattered across the basin, as the position of body A is not fixed.

For initial conditions of 0.4 m and 0 m/s, the system will behave as vibro-impact. The system will behave oscillatory for initial conditions of 0.45 m and 1.44 m/s (Figure 14).

The frequency for which this basin was obtained, is the one from range of frequencies for which the scatterings on amplitude-frequency diagrams (Figure 13) are noticed.

For this frequency and initial conditions, vibro-impact behavior of the system prevails, as shown by mentioned basin.

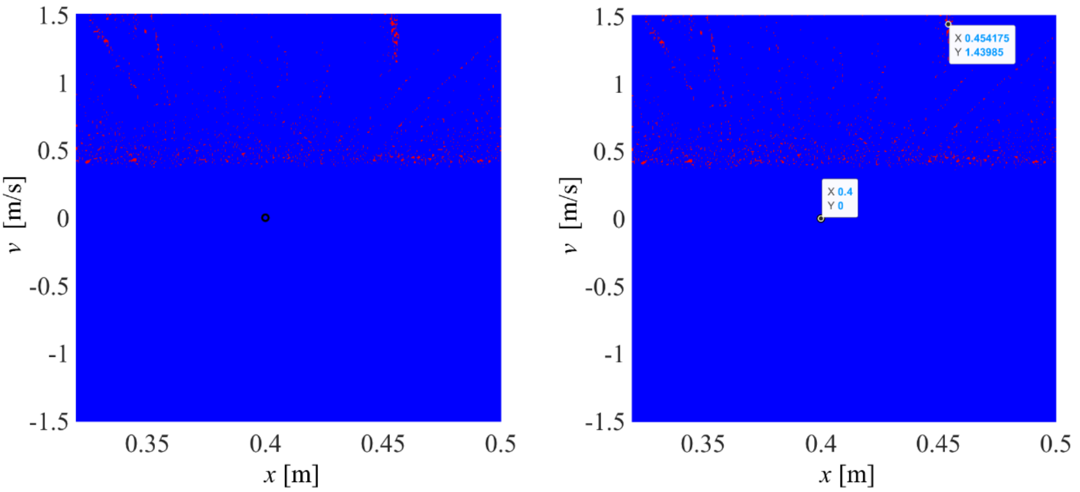

Figure 14. Basin of attraction of a ball, for Ω_p = 16 rad/s

Basin of attraction of the ball, for excitation frequency Ω_p = 22 rad/s, is shown in Figure 15. There are no noticed blue regions in this basin, for shown ranges of displacement and velocity of a ball.

This indicates that the behavior of the system is oscillatory, for all values of the initial conditions shown.

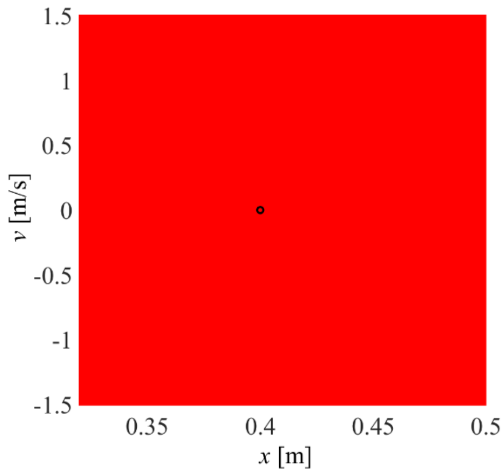

Figure 15. Basin of attraction of a ball, for Ω_p = 22 rad/s

4. Conclusion

In this paper, the behavior of a Duffing oscillator coupled with a vibro-impact element has been analyzed. Numerical simulations were performed for steady-state motion, and the results were presented in the form of amplitude–frequency diagrams, time–displacement diagrams and basins of attraction. Amplitude–frequency diagrams for jump-up and jump-down excitation frequencies were obtained.

Since Duffing and vibro-impact systems contain strong nonlinearities and motion stops, it is important to consider both simulations, as they may yield different solutions.

Scattering regions were observed in the amplitude–frequency diagrams for certain excitation frequencies.

Time–displacement diagrams showed that, for these frequencies, the motion of the system is chaotic.

It was also shown that, when the vibro-impact element is attached to the Duffing oscillator, the maximum amplitude of the main body is reduced and the resonance region shifts towards lower excitation frequencies.

The influence of the stiffness of the spring connecting the vibro-impact element to the oscillator was studied by comparing amplitude–frequency and time–displacement diagrams for several stiffness values. The maximum amplitude of the main body was found to be highest for the stiffest spring, while the scattering region in the amplitude–frequency diagrams became narrower as the stiffness increased. Consequently, a higher stiffness reduces the number of impacts of the ball and decreases the effectiveness of the vibro-impact element as an absorber; the system behaves more like a purely oscillatory one.

The system behavior also depends on the initial conditions. Basins of attraction were constructed for two selected excitation frequencies, one within a scattering region and one outside it. For the first frequency, the basins indicated that the response is predominantly vibro-impact, while for the second frequency the response is purely oscillatory.

In this study, attention was focused on steady-state behavior, and chaotic motion was detected for some excitation frequencies. A more detailed investigation of the chaotic dynamics of the Duffing oscillator coupled with a vibro-impact element is proposed as a subject of future work.

References:

[1]. Nayfeh, A. H., & Mook, D. T. (2024). *Nonlinear oscillations*. John Wiley & Sons.

[2]. Luo, A. C., & Guo, Y. (2013). *Vibro-impact dynamics*. John Wiley & Sons.

[3]. Kovacic, I., & Brennan, M. J. (2011). *The Duffing equation: nonlinear oscillators and their behaviour*. John Wiley & Sons.

[4]. El-Naggar, A. M., & Ismail, G. M. (2016). Analytical solution of strongly nonlinear Duffing oscillators. *Alexandria Engineering Journal*, *55*(2), 1581-1585.

[5]. Shamsi, M., & Razzaghi, M. (2004). Numerical solution of the controlled duffing oscillator by the interpolating scaling functions. *Journal of electromagnetic waves and applications*, *18*(5), 691-705.

[6]. Gandino, E., & Marchesiello, S. (2010). Identification of a duffing oscillator under different types of excitation. Mathematical Problems in Engineering, 2010(1), 695025.

[7]. Anh, N. D., & Hieu, N. N. (2012). The Duffing oscillator under combined periodic and random excitations. *Probabilistic Engineering Mechanics*, *30*, 27-36.

[8]. Piccirillo, V. (2021). Suppression of chaos in nonlinear oscillators using a linear vibration absorber. *Meccanica*, *56*(2), 255-273.

[9]. El-Ganaini, W. A. (2018). Duffing oscillator vibration control via suspended pendulum. *Appl. Math*, *12*(1), 203-215.

[10]. Beltran-Carbajal, F., Silva-Navarro, G., & Abundis-Fong, H. F. (2015). Application of Passive/Active Duffing Vibration Absorbers in Duffing Mechanical Systems. *Proceedings of the 22th International Congress on Sound and Vibration.*

[11]. Zhao, G., Raze, G., Paknejad, A., Deraemaeker, A., Kerschen, G., & Collette, C. (2020). Active nonlinear inerter damper for vibration mitigation of Duffing oscillators. *Journal of Sound and Vibration*, *473*, 115236.

[12]. Chatterjee, S., Mallik, A. K., & Ghosh, A. (1995). On impact dampers for non-linear vibrating systems. *Journal of Sound and Vibration*, *187*(3), 403-420.

[13]. Lampart, M., & Zapoměl, J. (2013). Dynamics of the electromechanical system with impact element. *Journal of sound and vibration*, *332*(4), 701-713.

[14]. Lizunov, P., Pogorelova, O., & Postnikova, T. (2024). Optimization of a vibro-impact damper design using MATLAB tools. *Strength of Materials and Theory of Structures*, (112), 3-18.

[15]. Li, T., Seguy, S., & Berlioz, A. (2017). Optimization mechanism of targeted energy transfer with vibro-impact energy sink under periodic and transient excitation. *Nonlinear Dynamics*, *87*(4), 2415-2433.

[16]. De Souza, S. L. T., et al. (2005). Impact dampers for controlling chaos in systems with limited power supply. *Journal of Sound and Vibration*, *279*(3-5), 955-967.

[17]. Chehaibi, K., Mrad, C., & Nasri, R. (2019). Collision modeling of single unit impact absorber for mechanical systems vibration attenuation. *Journal of Theoretical and Applied Mechanics*, *57*.

[18]. Li, H., Li, A., & Zhang, Y. (2021). Importance of gravity and friction on the targeted energy transfer of vibro-impact nonlinear energy sink. *International Journal of Impact Engineering*, *157*, 104001.

[19]. Gourc, E., et al. (2015). Quenching chatter instability in turning process with a vibro-impact nonlinear energy sink. *Journal of Sound and Vibration*, *355*, 392-406.

[20]. Kappagantu, R. (2008). Vibro-Impact Rotor Dampers For Brake Squeal Attenuation - Towards An Insulator Free Design To Quell Squeal. *SAE International Journal of Passanger Cars-Mechanical Systems*, *1*, 1188-1193.

[21]. Hajradinovic, D., Zukovic, M., & Kovacic, I. (2021). Numerical analysis of a vibro-impact system with ideal and non-ideal excitation. *Journal of Physics: Conference Series*, *1730*(1), 012014.

[22]. Babitsky, V. I. (2013). *Theory of vibro-impact systems and applications.* Springer.

[23]. Schmerr, L. W. (2019). Engineering Dynamics 2.0. *Cham: Springer Nature Switzerland*, *707*.

[24]. Ahmad, M., Ismail, K. A., & Mat, F. (2016). *Impact models and coefficient of restitution: A review*. *ARPN Journal of Engineering and Applied Sciences*, *11*(10), 6549–6555.